A&A 667, A106 (2022)
https://doi.org/10.1051/0004-6361/202244383

Astronomy & Astrophysics

Detecting H_2O with CRIRES+: WASP-20b*

M. C. Maimone[1,2], M. Brogi[3,4,5], A. Chiavassa[1,6], M. E. van den Ancker[2], C. F. Manara[2], J. Leconte[7], S. Gandhi[8,3,5], and W. Pluriel[9]

[1] Université Côte-d'Azur, Observatoire de la Côte d'Azur, CNRS, Lagrange, CS 34229 Nice, France
e-mail: maria-chiara.mmaimone@oca.eu
[2] European Southern Observatory, Karl-Schwarzschild-Str. 2, 85748 Garching, Germany
[3] Department of Physics, University of Warwick, Coventry CV4 7AL, UK
[4] INAF–Osservatorio Astrofisico di Torino, Via Osservatorio 20, 10025 Pino Torinese, Italy
[5] Centre for Exoplanets and Habitability, University of Warwick, Gibbet Hill Road, Coventry CV4 7AL, UK
[6] Max-Planck-Institut für Astrophysik, Karl-Schwarzschild-Straße 1, 85741 Garching, Germany
[7] Laboratoire d'astrophysique de Bordeaux, Univ. Bordeaux, CNRS, B18N, allée Geoffroy Saint-Hilaire, 33615 Pessac, France
[8] Leiden Observatory, Leiden University, Postbus 9513, 2300 RA Leiden, The Netherlands
[9] Département d'astronomie de l'Université de Genève, Chemin Pegasi 51, 1290 Versoix, Switzerland

Received 30 June 2022 / Accepted 22 September 2022

ABSTRACT

Context. Infrared spectroscopy over a wide spectral range and at the highest resolving powers ($R > 70\,000$) has proved to be one of the leading techniques to unveil the atmospheric composition of dozens of exoplanets. The recently upgraded spectrograph CRIRES instrument at the Very Large Telescope (CRIRES+) was operative for a first science verification in September 2021, and its new capabilities in atmospheric characterization were ready to be tested.
Aims. We analyzed transmission spectra of the hot Saturn WASP-20b in the K band (1981–2394 nm) that were acquired with CRIRES+ with the aim to detect the signature of H_2O and CO.
Methods. We used a principal component analysis to remove dominant time-dependent contaminating sources such as telluric bands and the stellar spectrum. We extracted the planet spectrum by cross-correlating observations with 1D and 3D synthetic spectra, without circulation.
Results. We present the tentative detection of molecular absorption from water vapor at a signal-to-noise ratio equal to 4.2 and 4.7 by using only H_2O 1D and 3D models, respectively. The peak of the cross-correlation function occurred at the same rest-frame velocity for both model types ($V_{\rm rest} = -1 \pm 1\,{\rm km\,s^{-1}}$) and at the same projected orbital velocity of the planet, but with different error bands (1D model: $K_{\rm P} = 131^{+18}_{-29}\,{\rm km\,s^{-1}}$; 3D: $K_{\rm P} = 131^{+23}_{-39}\,{\rm km\,s^{-1}}$). Our results agree with the result expected in the literature ($132.9 \pm 2.7\,{\rm km\,s^{-1}}$).
Conclusions. Although the observational conditions were not ideal and we had problems with the pipeline in calibrating and reducing our raw data set, we obtained the first tentative detection of water in the atmosphere of WASP-20b. We suggest a deeper analysis and additional observations to confirm our results and unveil the presence of CO.

Key words. planets and satellites: atmospheres – planets and satellites: individual: WASP-20b – techniques: spectroscopic – methods: data analysis

1. Introduction

The remote atmospheric characterization of exoplanets is a key milestone for unveiling their physical and chemical processes (Miller-Ricci et al. 2009), their formation history (Madhusudhan 2014; Eistrup et al. 2018), and ultimately, possible conditions suitable for life (Schwieterman 2016). In recent years, high-resolution spectroscopy ($R > 25\,000$) has become a tool at the forefront for acquiring exoplanet spectra. At high resolution, molecular bands are resolved into a forest of individual lines, which enables a line-by-line comparison with synthetic spectra through cross-correlation and allows disentangling the planetary signal, which is Doppler-shifted during the transit, from stationary or quasi-stationary signals, such as telluric bands and stellar spectral lines (Snellen et al. 2010).

The high demand in terms of signal-to-noise ratio for the characterization of exoplanets has always been the main limit of this technique. In past decades, a new generation of ground-based instruments have been built, however, to fulfill the minimum requirements in terms of resolution, stability, and adequate collective area to secure solid detections in the near-infrared. At infrared wavelengths, Very Large Telescope (VLT)/CRIRES has been the first successful instrument. It obtained the first detection of CO in transmission (Snellen et al. 2010) and the first detection of H_2O in emission (Birkby et al. 2013). Water was then confirmed with Keck/NIRSPEC by Lockwood et al. (2014), while Brogi et al. (2014) detected CO and H_2O simultaneously, and Brogi et al. (2016) provided a first measurement of winds and rotation, both results obtained with CRIRES. After CRIRES was decommissioned, other instruments were successful, starting with the detection of TiO via Subaru/HDS (Nugroho et al. 2017). Brogi et al. (2018) presented the first detection of CO+H_2O with TNG/GIANO, while Alonso-Floriano et al. (2019) found water in the J and Y bands of CAHA/CARMENES. In 2021, CHFT/SPIRou also presented detections of H_2O (Boucher et al. 2021) and CO (Pelletier et al. 2021). Giacobbe et al. (2021)

* Based on observations collected at the European Southern Observatory under ESO programme 107.22SX.001.

Table 1. Overview of WASP-20b observations during the first night of the science verification run of CRIRES+, as reported by the Paranal Differential Image Motion Monitor (DIMM).

Programme ID	107.22SX.001
Night	2021-09-16; 1:40UT–6:30UT
Phase	0.98–0.02
N_{obs}	75 (63 + 12)
Exp. time	1×180 s
Obs. mode	Nodding A-A-B-B-B-B-A-A
Slit	0.2″
AO loop	Closed
Max resolution	92 000
Wavelength setting	K2217 (1981–2394 nm)
Airmass	1.006–1.455
S/N	19–38 (AVG = 28)
Seeing (towards target)	0.82″–1.27″

Notes. N_{obs} is the total number of observed spectra, acquired before (63) and after (12) crossing the Zenith avoidance area. The exposure time is expressed as NDIT × DIT, where DIT is the detector integration time and NDIT is the number of detector integrations.

presented the simultaneous detection of six molecular species with GIANO, and Line et al. (2021) achieved the most precise abundance measurement to date with Gemini-S/IGRINS.

Recently, the CRIRES instrument has been upgraded into a cross-dispersed spectrograph (CRIRES+, Dorn et al. 2016) and started operating in September 2021. CRIRES+ allows high sensitivity in the infrared range (0.95–5.3 µm), where two main carriers of carbon (CO) and oxygen (H_2O) simultaneously imprint the spectrum (Madhusudhan 2012). Using CRIRES+, we observed WASP-20b during the science verification (SV) time of the instrument. Our goal was a demonstration of the basic capabilities of the new instrument, and we chose to observe WASP-20 because it was the only target with a visible transit during the SV observing window.

WASP-20b is a hot-Saturn in a 4.9-day near-aligned orbit around an F9-type star and has an equilibrium temperature of 1379 K. It was observed for the first time by Anderson et al. (2015), was discovered as a binary system separated by only 0.26″ by Evans et al. (2016), and was confirmed by Southworth et al. (2020).

In the following, we present the analysis of transmission spectra acquired with CRIRES+. They led us to the first tentative detection of water vapor in the atmosphere of WASP-20b.

2. Observations and data reduction

We observed WASP-20b for 5 h before, during, and after the 3.4-h transit that occurred on September 16, 2021. During the night, the target crossed the zenith-avoidance area of the telescope, causing a gap of 1 h in the acquisition. An overview of observations is shown in Table 1. We set the spectrograph to cover the wavelength range 1981–2394 nm (K-2217 band), roughly centered on the branch of 2-0 ro-vibrational transitions of carbon monoxide, where additional molecular absorption from water vapor, carbon monoxide, and methane is possible (Gandhi et al. 2020). We employed CRIRES+ at maximum resolution ($R = 92\,000$[1]) by using the 0.2″ slit. Target and sky spectra were taken with the nodding acquisition mode AABBBBAA for background subtraction. Although the airmass remained acceptable during the entire night (1.0–1.45) and the time-averaged seeing in the direction of the target did not exceed 1.27″, we obtained an averaged signal-to-noise ratio (S/N) of only 28. This value agrees with the value found by Holmberg & Madhusudhan (2022), but it turned out to be low when compared to other high-resolution observations (see Sect. 5 for details). We expected this to impact our final result negatively.

According to results from Evans et al. (2016) and Southworth et al. (2020), we also checked for traces of binarity by searching the vertical slices of our raw observations. We found no significantly resolved double peaks that could explain the presence of a second star. We therefore treated WASP-20 as a single star.

We performed the calibration and extraction of the spectra with the CRIRES+ pipeline (version 1.0.4, Valenti et al. 2021), ran through the esoreflex workflow (version 2.11.3, Freudling et al. 2013) and the command-line interface esorex (version 3.13.5)[2]. We used calibration frames that were acquired at the beginning of the night and just after the interruption for flat-fielding, dark-correction, wavelength calibration, and to take the nonlinearity between pixels and wavelengths into account. CRIRES+ is equipped with three detectors (CHIP1, CHIP2, and CHIP3), each of which is divided into eight orders. We successfully reduced and extracted raw spectra from orders 3, 4, 5, 6, and 7 of CHIP1 and orders 3, 4, 5, 6, 7, and 8 of CHIP2. The data reduction of all orders of CHIP3 and the eighth order of CHIP1 failed because the pipeline was unable to find the pixel-wavelength conversion tables (TraceWave tables) associated with these orders. Each full AABBBBAA nodding sequence (eight exposures) was combined at the level of the pipeline into a single reduced spectrum. At the end of the data reduction, we obtained 18 reduced spectra, 6 of them out of transit and 12 in transit. For our analysis, we used only in-transit spectra.

After the data reduction, we realized that the wavelength calibration performed with the pipeline was not accurate. In particular, the location of spectral lines at the edges of each order were clearly shifted farther than the spectral lines near the center of each order. We attempted to use our custom wavelength recalibration pipeline designed for the old CRIRES (Chiavassa & Brogi 2019) to realign the spectra. The code compares a telluric model with the data, and searches for a wavelength solution through Monte Carlo Markov chains. The higher the number of telluric absorption lines in a spectral range, the easier the comparison between the model and the data. Unfortunately, the calibration failed because of the lack of absorption lines within 2114–2140 nm and 2210–2222 nm. We had two options at this point: (1) use a principal component analysis (PCA) with spectra that were not aligned and preserve the original S/N, dealing with possible stellar contamination, or (2) remove these problematic orders (a total of 24 spectra), apply the technique developed by Chiavassa & Brogi (2019) to subtract stellar signal through 3D models and reduce stellar contamination before PCA, but risk to have insufficient planetary signal for a detection. We decided to proceed with the first option.

3. Methods: PCA and cross-correlation

At this initial stage of the analysis, ground-based high-resolution observations are dominated by telluric bands and the stellar spectrum, which are orders of magnitude stronger than the exoplanet

[1] Documented in the CRIRES user manual available at https://www.eso.org/sci/facilities/paranal/instruments/crires/doc.html

[2] Documentation available at the ESO website http://www.eso.org/sci/software/pipelines/

Table 2. System parameters from Anderson et al. (2015) compared to those used in this work as input for 1D and 3D models.

Parameters	Anderson et al. (2015)	Inputs models This work
M_P (M_J)	0.311 ± 0.017	0.311
R_P (R_J)	1.462 ± 0.059	1.462
T_{eq} (K)	1379 ± 31	1400
g (m s^{-2})	3.36 ± 0.28	3.77
p (bar)	–	10^2–10^{-8} (1D) 2×10^2–10^{-9} (3D)

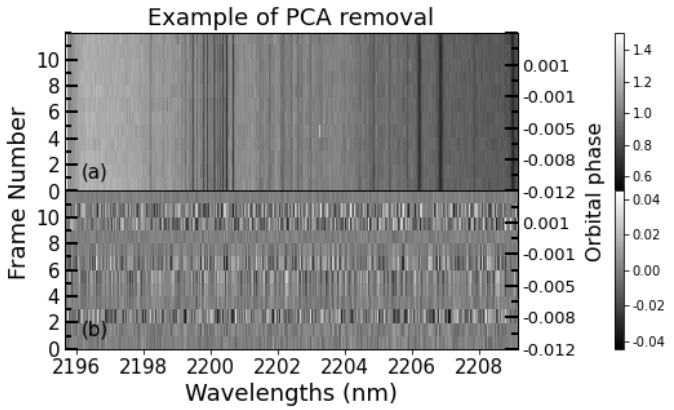

Fig. 1. Example of PCA removal from WASP-20 data, observed during the first night of the SV time with CRIRES+. The sequence of 12 normalized spectra is shown in the wavelength range 2195–2209 nm (fifth order of CHIP1) before (*panel a*) and after (*panel b*) the removal of the first seven principal components.

signals of interest and therefore can be considered as contaminant signals in the study of exoplanetary atmospheres. To extract the planetary spectrum, we executed the two steps described below as done in Giacobbe et al. (2021):

1. Principal component analysis (PCA)
2. Cross-correlation.

The PCA can identify and remove the dominant time-dependent contaminating sources that are quasi-stationary in wavelength, such as telluric bands (vertical black lines in Fig. 1a), stellar lines, and systematic trends caused by instruments, and leave the planet signal and the uncorrelated noise as residuals (Fig. 1b). Typically, the number of removed components varies between two and eight, depending on the quality of the data (Giacobbe et al. 2021). Before applying the PCA, we corrected the raw spectra for detector cosmetics and cosmic rays by substituting bad pixels with NaN strings. This facilitated the later masking of bad pixels in the analysis.

The spectra were normalized by their median value to correct for changes in the overall amount of flux that reaches the detectors due to variable transparency, imperfect telescope pointing, or instability of the stellar point spread function. Subsequently, we subtracted the mean from each spectral channel (each column) and divided each spectrum (each row) by its standard deviation. The spectra were given as input to the singular value decomposition (SVD) Python function numpy.linalg.svd[3]. The output was a matrix of eigenvalues, extracted for a given number of components. We performed a multilinear regression between the eigenvalues found via SVD and the matrix of fluxes after median normalization, and we divided the latter by the resulting fit. Last, a high-pass Gaussian filter with a FWHM of 80 pixels was applied to the data, and residual outliers were masked.

The Cross-correlation of WASP-20b data with transmission synthetic spectra to extract the planet signal. Even if a single absorption line has an $S/N \ll 1$, there are hundreds of strong molecular lines in the CRIRES+ K band. By coadding them into a single cross-correlation function (CCF), the faint signal of the planet is enhanced by a factor of approximately $\sqrt{N_{\rm lines}}$ (Brogi et al. 2014), allowing us to attempt a detection of the planet signature.

Because we did not resolve the binary nature of WASP-20 found by Evans et al. (2016) and Southworth et al. (2020) with CRIRES+, we treated the system as a single star (as noted in Sect. 2) and took Anderson et al. (2015) as main reference. The final result is strictly related to this choice: different planetary mass and radius reflect on the differences in surface gravity and atmospheric pressure, which have direct consequences on the atmospheric molecular absorption and on the shape of the planetary spectrum that we cross-correlated with the data.

We used synthetic spectra computed from 1D models using GENESIS (Gandhi & Madhusudhan 2017) and from SPARC/MIT Global Circulation Models (GCM, Showman et al. 2013; Parmentier et al. 2021; Pluriel et al. 2022) using Pytmosph3R (Caldas et al. 2019; Falco et al. 2022). We selected the GCMs that were closest to WASP-20b in terms of mass, radius, and temperature (see Table 2), and we used the same values to calculate 1D models. Only the pressure ranges were slightly different. We chose 3D GCMs that did not include dynamics (i.e., planet rotation, circulation, and winds) to make the comparison of 1D and 3D as plain as possible. In this way, the changes in line shape and intensity can be ascribed only to the inherent 3D structure of the planet T-p profile. All models were computed with an isothermal profile of 1400K, without thermal inversion or clouds. We first assumed solar metallicity and computed abundances at chemical equilibrium for all the species. Then we included only CO and H_2O in the final models we used in our analysis. As shown by Gandhi et al. (2020), at 1400K and at 2.3 µm, CO and H_2O are the dominant sources of opacities. We therefore computed three synthetic spectra per each model type, containing (i) only CO molecules, (ii) only H_2O, and (iii) CO+H_2O (Fig. A.1). The CO opacities of GCMs and H_2O opacities of both model types were taken from the ExoMol database (Polyansky et al. 2018), while CO opacities of 1D models were taken from the HITEMP database (Li et al. 2015). We assumed the same volume mixing ratio (VMR) for water vapor in both model types ($\log[H_2O] = -3.3$), but for CO, the VMR was slightly different ($\log[CO] = -3.4$ and -3.35 in 1D and 3D models, respectively). A summary is given in Table 2 and in Fig. A.1.

4. Results

Following the method explained in Sect. 3 step by step, we obtained the results shown in Fig. 2. The six figures represent the total strength of the cross-correlation signal as a function of the planet rest-frame velocity $V_{\rm rest}$ and the projected orbital velocity K_P calculated by using only H_2O (a, d), only CO (b, e), and $H_2O + CO$ (c, f) 1D models (top row) and 3D GCM models (bottom row).

[3] Available at https://numpy.org/doc/stable/reference/generated/numpy.linalg.svd.html

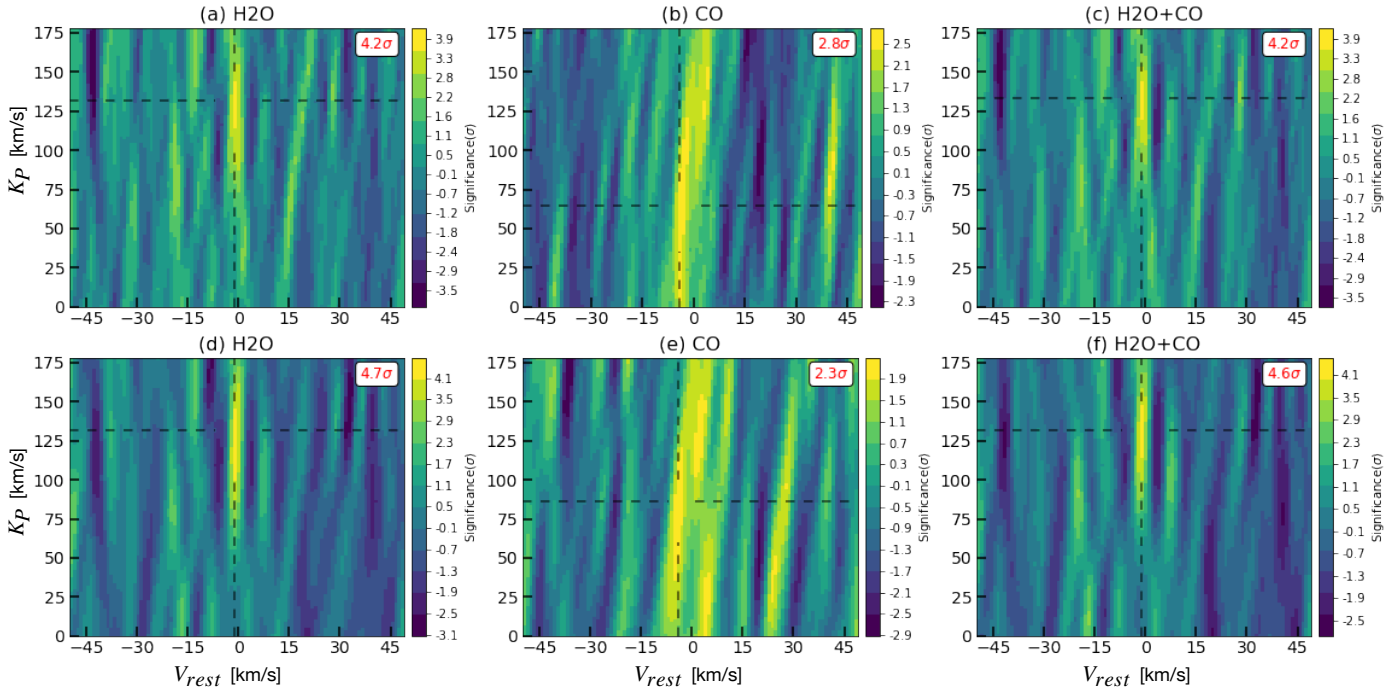

Fig. 2. Total cross-correlation signal from only H_2O (*panels a and d*), only CO (*panels b and e*), and $H_2O + CO$ (*panels c and f*) for the atmosphere of WASP-20b, shown as a function of rest-frame velocity and planet-projected orbital velocity. 1D models were used in the top row, and 3D GCM models were in the *bottom row*. Both model types are cloud free, in chemical equilibrium, and without thermal inversion. They contain a VMR equal to −3.3 for H_2O and to −3.4 and −3.5 for CO in the 1D and 3D models, respectively.

Water vapor is detected with both 1D and 3D only H2O models at an S/N of 4.2 and 4.7, respectively, after removing the first seven principal components with the PCA. The level of detection was estimated by dividing the peak value of the cross-correlation by the standard deviation of the noise. The peak occurred in correspondence of the same velocities for both model types, but with different error bars for K_P: $V_{rest} = -1 \pm 1\,km\,s^{-1}$, $K_P = 131^{+18}_{-29}\,km\,s^{-1}$ with the 1D model, and $K_P = 131^{+23}_{-39}\,km\,s^{-1}$ with the 3D model.

We compared our results with the RV semi-amplitude expected from the results of Anderson et al. (2015). We calculated the orbital velocity $V_{orb_A} = \frac{2\pi a}{P} = (133.3 \pm 1.5)\,km\,s^{-1}$ and obtained a $K_{P_A} = V_{orb_A} \sin i_A = (132.9 \pm 2.7)\,km\,s^{-1}$, which agrees with both our 1D and 3D K_P values.

No significant cross-correlation signal was obtained for carbon monoxide ($S/N < 3$) with the chosen models. The peak seems rather split and spread over a wide range of K_P, with the maximum shifted toward lower K_P (86 and 64 $km\,s^{-1}$ with the 1D model and GCM, respectively) and negative V_{rest} ($-4\,km\,s^{-1}$ in both cases). It is possible that this is caused by a strong contamination from CO absorption lines of the star that is left in the residuals during the PCA. The cross-correlation with the $H_2O + CO$ models reflects the signature of water vapor, but with a lower S/N level (4.2 and 4.6) due to the pollution of the CO contribution.

We determined the statistical significance of the H_2O signal as in previous work (Brogi et al. 2012, 2013). From the matrix containing the cross-correlation signal as a function of planet radial velocity and time, CCF(V, t), we selected the values that do not belong to the planet RV curve (out of trail) and those that belong to the planetary trace (in trail). In Fig. A.2, we show histograms made of out-of-trail values with a solid yellow line and those made of in-trail values with a solid blue line, obtained with the 1D model (left panel) and 3D (right panel) model. The distribution of the cross-correlation noise is clearly centered at zero and the distribution containing the planet signal is systematically shifted toward higher values. This can be tested statistically by using a Welch t-test. For the signal from WASP-20b, we were able to reject the hypothesis that the out-of-trail and in-trail distributions are drawn from the same parent distribution at a 3.1σ level of confidence for the 1D model and at a 4.1σ level for the 3D model (see Fig. A.2).

5. Discussion and conclusions

We reported the first tentative detection of water vapor in the atmosphere of WASP-20b that was made through the recently upgraded spectrograph CRIRES+. No significant peak was found for carbon monoxide, likely due to a considerable contamination from stellar absorption.

Our H_2O detection significance (3.1σ with the 1D model and 4.1σ with 3D model) is slightly lower than the significance that was achieved with other instruments in the literature, which always observed the object in transmission: Brogi et al. (2016), for instance, detected H_2O in the atmosphere of HD 189733b with a statistical significance equal to 4.8σ in the same band as we did with VLT/CRIRES, Alonso-Floriano et al. (2019) and Sánchez-López et al. (2019) found water vapor at 7.5σ in HD 189733b and and 8.1σ in HD 209458b, both around 1.15 and 1.4 µm with CAHA/CARMENES, and Giacobbe et al. (2021) also detected water vapor in HD 209458b, but at 9.6σ in the range 0.95–2.45 µm with TNG/GIARPS. However, a crucial difference between our observations and the other ones is the initial S/N: for example, Giacobbe et al. (2021) measured a mean S/N between ∼80 and ∼120 per spectrum per pixel averaged across the entire dataset and the entire spectral range; the

typical continuum S/N per spectrum reached in Alonso-Floriano et al. (2019) was ~150; the mean S/N for Sánchez-López et al. (2019) was ~85 for the bands at 1.15 µm and ~65 for the band at 1.4 µm in the first half of the observations, even though it dropped to below 60 and 50, respectively, in the second half. We were unable to find information about the S/N of observations in Brogi et al. (2016). In contrast, our observations reached a mean of only 28 (see Sect. 2 and Table 1).

A thorough and accurate comparison with other observations might have shed light on the causes of the lower S/N (e.g., whether it was due only to the instrument, only to the particular target choice, or to a combination of both), but a comparison like this was beyond the purpose of this work. However, we tried to identify potential weaknesses that are to be avoided or corrected for in the future. For example, an incorrect NDIT (NDIT = 2 instead of 1) was chosen during the preparation of these observations, causing a halving of temporal resolution. Moreover, during the night, the target crossed the zenith avoidance area, resulting in an observational gap of 1 h and in a loss of one-third of the planetary transit. Future observations should consider a different period to avoid the gap. In addition, the pipeline that we used failed in reducing more than one-third of the dataset (all orders of CHIP3 and the eighth order of CHIP1) and was inaccurate in the wavelength solution. Particularly for the CO, this prevented us from correcting the dataset for stellar contamination, which, as done in Caldas et al. (2019) and Flowers et al. (2019), can increase the significance and allow a clearer detection.

Future deeper analyses should first aim at refining the wavelength solution by using the updated version of the pipeline and correct for the spectrograph instability at the subpixel level. Future observations are equally strongly suggested to improve our preliminary results. The more efficient ABBA nodding pattern should be preferred to gain in temporal resolution. The S/N of CO of WASP-20b might be noticeably increased by observing at longer wavelengths of CRIRES+ close to 4.5 µm (de Kok et al. 2014), for instance.

Acknowledgements. This project has been developed during an ESO Studentship (M.C.M.) and has received funding from the European Research Council (ERC) under the European Union's Horizon 2020 research and innovation programme (grant agreement no. 679030/WHIPLASH (M.C.M.); and project FOUR ACES, grant agreement no. 724427 (W.P.)). It has also been carried out in the frame of the National Centre for Competence in Research PlanetS supported by the Swiss National Science Foundation (SNSF) (W.P.). W.P. acknowledges financial support from the SNSF for project 200021_200726. M.B. acknowledges support from the UK Science and Technology Facilities Council (STFC) research grant ST/T000406/1. J.L. also acknowledges funding from the french state: CNES, Programme National de Planétologie (PNP), the ANR (ANR-20-CE49-0009: SOUND). For this work, it was granted access to the HPC resources of Observatoire de la Côte d'Azur – Mésocentre SIGAMM. This research made use of IPython, Numpy, Matplotlib, SciPy, and Astropy[4], a community-developed core Python package for Astronomy (Astropy Collaboration 2013).

References

Alonso-Floriano, F. J., Sánchez-López, A., Snellen, I. A. G., et al. 2019, A&A, 621, A74
Anderson, D. R., Collier Cameron, A., Hellier, C., et al. 2015, A&A, 575, A61
Astropy Collaboration (Robitaille, T. P., et al.) 2013, A&A, 558, A33
Birkby, J. L., de Kok, R. J., Brogi, M., et al. 2013, MNRAS, 436, L35
Boucher, A., Darveau-Bernier, A., Pelletier, S., et al. 2021, AJ, 162, 233
Brogi, M., Snellen, I. A. G., de Kok, R. J., et al. 2012, Nature, 486, 502
Brogi, M., Snellen, I. A. G., de Kok, R. J., et al. 2013, ApJ, 767, 27
Brogi, M., de Kok, R. J., Birkby, J. L., Schwarz, H., & Snellen, I. A. G. 2014, A&A, 565, A124
Brogi, M., de Kok, R. J., Albrecht, S., et al. 2016, ApJ, 817, 106
Brogi, M., Giacobbe, P., Guilluy, G., et al. 2018, A&A, 615, A16
Caldas, A., Leconte, J., Selsis, F., et al. 2019, A&A, 623, A161
Chiavassa, A., & Brogi, M. 2019, A&A, 631, A100
de Kok, R. J., Birkby, J., Brogi, M., et al. 2014, A&A, 561, A150
Dorn, R. J., Follert, R., Bristow, P., et al. 2016, SPIE Conf. Ser., 9908, 99080I
Eistrup, C., Walsh, C., & van Dishoeck, E. F. 2018, IAU Symp., 332, 69
Evans, D. F., Southworth, J., & Smalley, B. 2016, ApJ, 833, L19
Falco, A., Zingales, T., Pluriel, W., & Leconte, J. 2022, A&A, 658, A41
Flowers, E., Brogi, M., Rauscher, E., Kempton, E. M. R., & Chiavassa, A. 2019, AJ, 157, 209
Freudling, W., Romaniello, M., Bramich, D. M., et al. 2013, A&A, 559, A96
Gandhi, S., & Madhusudhan, N. 2017, MNRAS, 472, 2334
Gandhi, S., Brogi, M., Yurchenko, S. N., et al. 2020, MNRAS, 495, 224
Giacobbe, P., Brogi, M., Gandhi, S., et al. 2021, Nature, 592, 205
Holmberg, M., & Madhusudhan, N. 2022, AJ, 164, 79
Li, G., Gordon, I. E., Rothman, L. S., et al. 2015, ApJS, 216, 15
Line, M. R., Brogi, M., Bean, J. L., et al. 2021, Nature, 598, 580
Lockwood, A. C., Johnson, J. A., Bender, C. F., et al. 2014, ApJ, 783, L29
Madhusudhan, N. 2012, in EGU General Assembly Conference Abstracts, EGU General Assembly Conference Abstracts, 13720
Madhusudhan, N. 2014, in American Astronomical Society Meeting Abstracts, 223, 207.02
Miller-Ricci, E., Seager, S., & Sasselov, D. 2009, in Transiting Planets, eds. F. Pont, D. Sasselov, & M. J. Holman, 253, 263
Nugroho, S. K., Kawahara, H., Masuda, K., et al. 2017, AJ, 154, 221
Parmentier, V., Showman, A. P., & Fortney, J. J. 2021, MNRAS, 501, 78
Pelletier, S., Benneke, B., Darveau-Bernier, A., et al. 2021, AJ, 162, 73
Pluriel, W., Leconte, J., Parmentier, V., et al. 2022, A&A, 658, A42
Polyansky, O. L., Kyuberis, A. A., Zobov, N. F., et al. 2018, MNRAS, 480, 2597
Sánchez-López, A., Alonso-Floriano, F. J., López-Puertas, M., et al. 2019, A&A, 630, A53
Schwieterman, E. W. 2016, Ph.D. Thesis, University of Washington, Seattle, USA
Showman, A. P., Fortney, J. J., Lewis, N. K., & Shabram, M. 2013, ApJ, 762, 24
Snellen, I. A. G., de Kok, R. J., de Mooij, E. J. W., & Albrecht, S. 2010, Nature, 465, 1049
Southworth, J., Bohn, A. J., Kenworthy, M. A., Ginski, C., & Mancini, L. 2020, A&A, 635, A74
Valenti, E., Brucalassi, A., & Rodler, F. 2021, CRIRES User Manual, avalaible at https://eso.org/sci/facilities/paranal/instruments/crires/doc.html

[4] Available at http://www.astropy.org/

Appendix A:

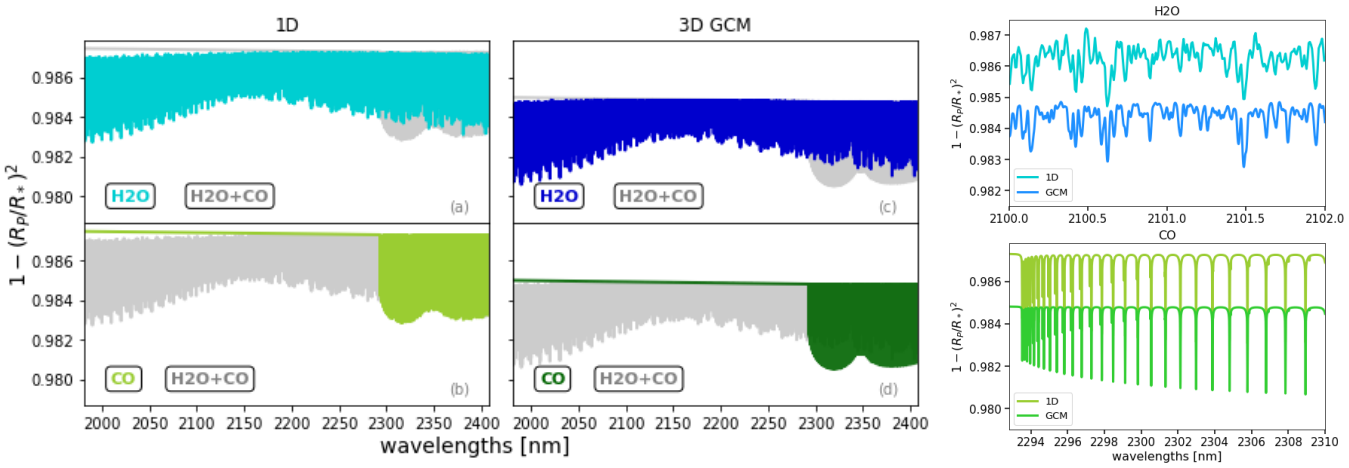

Fig. A.1. All models used in this work (see Sec. 3 for details), represented as the flux received from the star during transit relative to the out-of-transit stellar flux as a function of wavelengths (left). From left to right, we show the 1D models [panels (a) and (b)] and GCMs [panels (c) and (d)]. In each plot, the gray line plots the model in which both molecular species were studied in this work, i.e., water and carbon monoxide. Only H_2O [panels (a),(c)] and only CO [panels (b),(d)] models are overplotted with blue and green colors, respectively, in the top and bottom panels. Overall, GCMs (darker colors) have a deeper absorption than the 1D models (lighter colors) due to a different starting pressure at the bottom of the atmosphere. A zoom over a smaller wavelength range of only H_2O (top panel) and only CO (bottom panel) 1D and 3D models is shown (right).

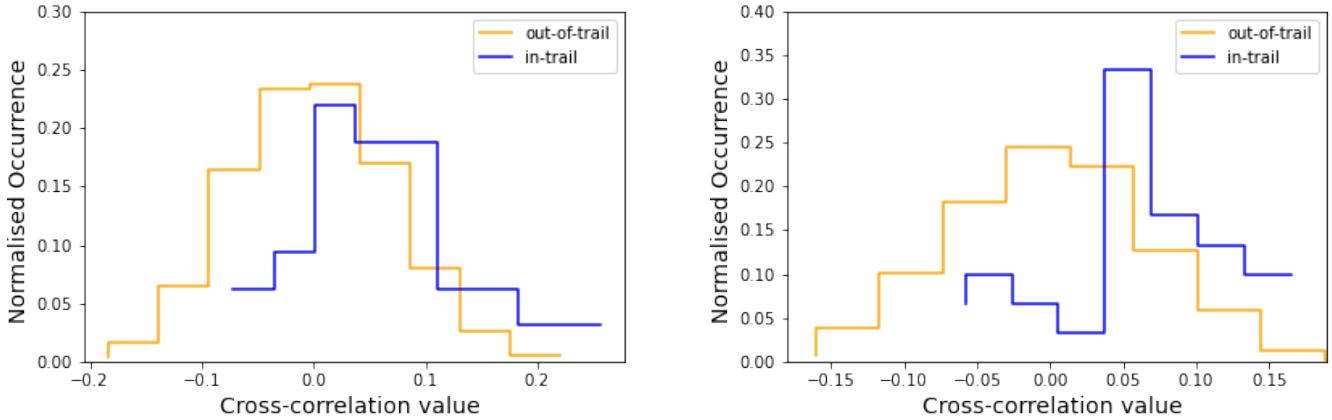

Fig. A.2. Comparison between the distribution of cross-correlation values outside (solid yellow line) and inside (solid blue line) the radial velocity trail of WASP-20b obtained with the only H_2O 1D model (left panel) and 3D model (right panel).